Mesh Addition Based on the Depth Image (MABDI)

by

Lucas E. Chavez

B.S., Mechanical Engineering
New Mexico Institute of Mining and Technology, 2009

THESIS

Submitted in Partial Fulfillment of the
Requirements for the Degree of

Master of Science
Mechanical Engineering

The University of New Mexico

Albuquerque, New Mexico

December, 2016

Acknowledgments

This work was support in part by Sandia National Laboratories under Purchase Order: 1179196 and NSF grant OISE #1131305.

Mesh Addition Based on the Depth Image (MABDI)

by

Lucas E. Chavez

B.S., Mechanical Engineering
New Mexico Institute of Mining and Technology, 2009

M.S., Mechanical Engineering, University of New Mexico, 2016

Abstract

Many robotic applications, especially those whose goal is to aid or assist through human-robot interaction, utilize a rich map of the world for reasoning tasks such as collision detection, path planning, or object recognition. Such map, and the method used to produce it, must take into consideration real-world constraints. Most mesh-based mapping algorithms resemble a "black box" and do not provide a mechanism to close the loop and make decisions about the incoming information. MABDI leverages the global mesh by finding the difference between what we expect to see and what we are actually seeing, and using this to classify the incoming measurements as novel or not. This allows the surface reconstruction method to be run only on data that has not yet been represented in the global mesh. The result is an algorithm that becomes computationally inexpensive once the environment is known, but can also react to new objects.

Contents

Chapter 1

Introduction

1.1 Overview

Many robotic applications, especially those that involve human-robot interaction, often require a rich representation of the environment in order to perform such behavior as path planning and obstacle avoidance. In general, a rich representation, or map, is useful for providing situational awareness to an autonomous agent. A map is also important for applications such as teleoperation [1].

In robotics, map building in an unknown environment is referred to as the Simultaneous Localization and Mapping (SLAM) problem [2]. This label describes the fact that a methodology which solves the SLAM problem must simultaneously locate the robot in the environment as well as map the environment. The focus of this work is the mapping aspect of the SLAM problem. Fig. 1.1 gives a visualization of the goal.

The methodology to build a map is a continuously evolving subject in the field of robotics and computer graphics. Well known works of map building methods be-

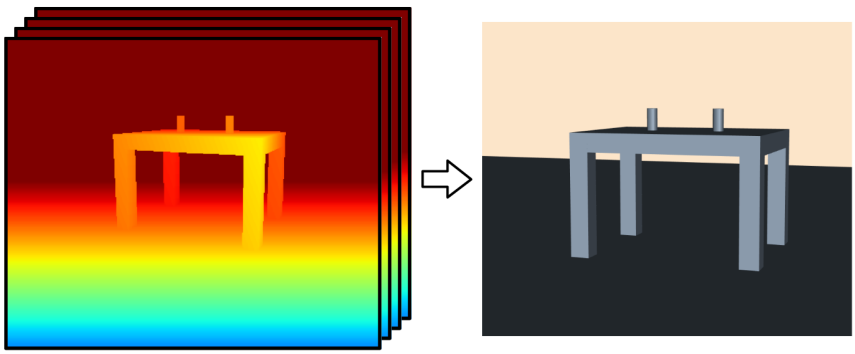

Figure 1.1: Goal is to create a map from depth images.

gan to be seen around 1987 [3]. Since then, the methods and the representations themselves have continued to evolve at an impressive rate. Growth in this field of research has been fueled by continuous advances in computing and sensing technologies. Over the years, sensors have continued to generate measurements at higher rates, higher resolution, and lower cost. RGB-D sensors are a new category of sensor that have recently gained extensive popularity in the robotics community due to their affordability and ability to generate a rich amount of data.

1.1.1 RGB-D Sensors

The popularity of RGB-D sensors began with the release and commercialization of the Kinect^{TM} by Microsoft. The arrival of the Kinect brought with it an inexpensive depth sensor that uses an active range system to generate a depth map of a given environment [4]. The Kinect and similar sensors, have come to be called RGB-D sensors. This class of sensors provide images which include both visual (RGB) and depth (D) values. Several works have taken advantage of this sensor technology in scenarios such as environmental mapping [5], 3D reconstruction [6], gesture recognition [7], and altitude control of aerial vehicles [8].

RGB-D sensors generally provide data at 30 frames per second and 640×480 resolution. Consequently, methods that use RGB-D data must handle over 9 million pixel values per second, if only using the depth information (D), and over 18 million if using both color (RGB) and depth (D). The magnitude of the amount of data output from RGB-D sensors create the need for mapping methods that are computationally inexpensive and also influence the type of data structure used to store the map.

1.1.2 Maps

There are different types of data structures that can define a map. All types have both intrinsic characteristics that impact the algorithms that generate them and constraints that must be considered for real-world applications. In addition, we are concerned with rich representation types, in contrast to sparse representation types [9], because rich types have the most use in applications such as human-robot interaction.

Table 1.1: Comparison of constraints for different map types.

	Supported	Computationally Inexpensive	Low Memory Requirement
Point Clouds	x	x	-
Surfels	-	x	x
Implicit Functions	x	-	-
Mesh	x	x	x

When considering which type of map is best for real-world applications, we must consider the constraints imposed by each type:

- Supported - Is there software, tools, research, algorithms, etc., for this type of map?

- Computationally Inexpensive - Can the algorithms run quickly on low cost computers (rather than specialized hardware)?
- Low Memory Requirement - Can the algorithms run on hardware with a standard amount of RAM?

Table 1.1 compares the constraints of common map types. We can see, in general a mesh type map satisfies real-world constraints. Additionally, It has been used extensively by the gaming and graphics communities, and so benefits from an incredible amount of continued research and advances in hardware such as Graphics Processing Units (GPUs).

1.2 Goal

The goal of this work is to develop a mapping algorithm that can gracefully utilize the amount of data output from an RGB-D sensor. Additionally, the algorithm will make use of software tools and hardware that have been developed for mesh data structures. The algorithm will be able to make intelligent decisions on the data it receives based on the knowledge it has been building about the environment. The decisions will be driven by the leveraging the difference between what the algorithm is actually seeing and what it expects to see. The decisions will be generated using computationally inexpensive computer vision methods.

1.3 Contribution

Currently, one of the issues with mesh mapping techniques is they are generally "black box" methods. Meaning the data comes in from the sensor, those measurements are turned into a mesh, and then that mesh is appended to a global mesh.

Fig. 1.2 visualizes this common pipeline in black. The goal of this work is to design an algorithm to close the loop (as visualized in red) and allow the system to make decisions about the incoming data based on what it already knows.

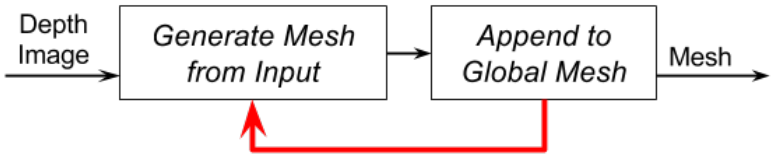

Figure 1.2: Common "black box" pipeline in black. The contribution of MABDI in red.

Chapter 2

Related Works

A major problem in robotics has been and continues to be: How can we create the "best" representation of an unknown environment? There are two main communities of researchers who been working on developing algorithms and methods to answer precisely this question. They are the robotics community and the computer graphics community and each community has a slightly different motivation for solving this problem. The robotics community is concerned with developing a real-time solution of generating representations in large environments. These representations are used by both fully autonomous and teleoperated systems. The common name which is used by the robotics community for this problem is Simultaneous Localization and Mapping or SLAM. The name SLAM refers to the problem of mapping and locating a robot in an unknown environment. Early methods generated very sparse representations of the world, as time and sensor technology progressed the representations became denser. A dense representation is desired for any system which must have good situational awareness of its environment. The computer graphics community is concerned with generating high quality representations of smaller environments and single objects. They generally refer to the problem as surface reconstruction. These representations are used by augmented reality, computer game object creation, 3D

printing, and more applications. In the following sections we will trace the development of representation generating methods in both communities. We will then discuss what is needed in future work.

2.1 SLAM

The problem of SLAM has been a primary focus of the robotics community for more than 25 years. A complete solution to the SLAM problem must be able to generate a representation of an unknown environment and track the robot in this new representation. In this body of literature the act of generating a representation is referred to as mapping. A good overview of the problem can be found in [10] and [11]. Each solution is designed to consider the goal application, type of sensor, computational constraints, and memory limits. All these factors influence the researcher's choice of what type of representation to use for the mapping procedure. In 2002 Thrun wrote a famous survey [2] of the SLAM literature which categorized existing algorithms on many traits including the representation. The representation choice of prior work can be roughly categorized into 3 types. The first type is characterized by some sort of list of 2D or 3D points and are usually considered to be sparse representations. Common names for these types are landmark locations and point clouds. The second type are considered to be more volumetric based and are often times considered to be a dense representation. Common names for these types are occupancy grid and Truncated Signed Distance Function (TSDF). The last type have the characteristic of being a surface representation and are also considered to be a dense representation. Common names for these types are surfels and mesh. In the following sections we will trace the history of each of the 3 types of representation that is seen in the SLAM literature.

2.1.1 Point Locations

One of the most well known and earliest solution to the SLAM problem, which uses a point location representation, was proposed by Smith et al. in 1990 [12]. The mathematical framework that he created was the origin of a family of solutions based on the Extended Kalman Filter (EKF). The representation he chose was simply a list of 2D landmark locations. Each location was part of a state matrix which was estimated at every iteration. A list of landmark locations was chosen because it allowed the method to have a low computational cost and use a small amount of memory, important factors in the days of early computing. There have been many improvements to the family of SLAM solutions which generate a list of point locations since Smith's work. One of the first practical implementations on a real robot was done by Thrun in 1998 [13]. In this work the SLAM problem was posed in an Expectation Maximization (EM) framework which is similar to the EKF framework in that landmark locations are saved in a state vector which is estimated at every iteration. In Thrun's work an occupancy grid map is generated as a post processing step from sonar measurements. The results showed that their representation could become more accurate over time by using new observations to improve the current estimate. This a highly desired ability of any representation generation method. The next step was the ability of these methods to include a loop closure procedure. A loop closure procedure was proposed by Gutmann in 1999 [14]. The key ability of the method was it could recognize when the robot was revisiting a prior location and adjust the entire representation with the constraint that the two points must coincide. In 2001 Dissanayake et al. [9] derived 3 theorems to theoretically prove the convergence of the SLAM problem. Their test platform used a millimeter-wave radar mounted on a vehicle and generated a list of 2D landmark locations. In 2001 Thrun et al. [15] cast the SLAM problem using particle filter techniques. Their results generated a 2D map and showed an increased robustness and lower computational

cost than prior methods. One of the key disadvantages of methods up to this point was that complexity scaled quadratically with the number of landmark locations. In 2002 Montemerlo et al. [16] created a SLAM solution named FastSLAM which was able to handle a much larger number of landmarks. They showed results with maps containing more than 50,000 points. Then, SLAM solutions using point locations became much more directed towards 3D.

Some of the first interesting works which represented the world as a list of 3D point locations were done by Thrun et al. in 2000 [17], Liu and Emery in 2001 [18], and Hähnel et al. in 2003. In these works the 2D landmark locations and robot position were estimated using very similar techniques from past work. Once this had been done the 3D laser scan data was simply appended to each estimated robot location. Then, a mesh was created by post processing the 3D point cloud. They utilized the fact that the laser collected the data in an incremental manner and simply connected neighboring 3D points. Finally, the mesh was simplified by looking for large planar sections and merging the corresponding mesh elements. One of the first SLAM solutions which used a single camera to generate a list of 3D points was done by Davison in 2003 [19]. Here he used a single camera to generate a very sparse list of 3D points. This method was limited to small environments. Future advances allowed representations of larger environments. In 2003 Thrun et al. [20] created a SLAM procedure which did not rely on having a structured environment and was applied to mapping large mines. In 2004 Howard et al. [21] created a SLAM systems based on a Segway platform equipped with a 3D laser which could map large areas of roughly 0.5 km on each side. One of the results showed a map with approximately 8 million points. In 2006 Cole and Newman [22] continued work in large-scale SLAM by increasing robustness and also generated maps with many 3D points using a laser sensor. In 2007 Clemente et al. created a large-scale SLAM system that used a single camera. The system had an advanced loop closing procedure based on visual features and created large maps of 3D points. In 2001 Klein and Murray [23] developed a

SLAM solution which used a single camera. The uniqueness of their method was the algorithmic structure. Their SLAM solution consisted of 2 separate processes: a tracking processes and a map building process. This algorithmic structure has become very common in many current SLAM solutions because of the advances in pose estimation technology. Klein and Murray were able to get very good results for a small environment and showed Augmented Reality (AR) applications. Many of the future advances of SLAM solutions, which generated 3D point sets, dealt with camera systems [24, 25, 26] and improved in speed and robustness. Many of the most current methods which produce a list of points are systems that use a relatively new type of sensor named a RGB-D sensor. One good example is a work that was produced in 2011 by Engelhard et al. [27]. In this work they used an algorithm named the Iterative Closest Point (ICP) [28] to align point clouds from coming from the RGB-D sensor into a large colored point cloud. The resulting maps were visually impressive. However, the map could not be adapted to new information and was not well suited for other applications, such as obstacle avoidance. These limitations are inherent in maps that consist of lists of points.

2.1.2 Volumetric

Many SLAM solutions generate a 2D volumetric representation of the world because they are especially advantageous in dealing with noisy sensors. Two of the first major works which generated a 2D volumetric representation were done in 1998 by Yamauchi et al. [29] and Schultz et al. [30]. These works generated a 2D occupancy grid which is a type of volumetric representation. Here the environment was divided into a 2D grid. Each square of the grid contained the probability that it was occupied with an object. All squares would be updated iteratively based on the current sensor readings. Occupancy grids, like any other volumetric-based representation, are limited by the amount of available memory. In 2002 Biswas et

al. [31] extended occupancy grid methods by allowing dynamic environments. This was done by looking at past "snapshots" of the map. In 2004 Eliazar and Parr [32] continued the advancement by decreasing computational cost and implemented a loop closure method.

There have been a few impressive SLAM solutions which generate a 3D volumetric representation. There are three major works which generated something very similar to a 3D occupancy grid which was saved as in a octree data structure [33, 34, 35, 36]. Each work had a slightly different name and procedure for generating the representation, but in general the representations divided the environment into cubes and had a scalar value representing the belief of a surface being there. Octrees were used to save memory by only having a fine resolution of cubes at places where there was a surface. There are many advantages to a 3D occupancy grid representation. When applied to obstacle avoidance and path planning algorithms. Also, the representation is very adaptable to new information. The major disadvantage is that the representation can not be visualized immediately. In order to render, an image must be generated at each desired viewpoint by ray tracing the volume. This can be a problem when using such method for applications such as teleoperation due to the computational cost of rendering. The current state of the art for generating a volumetric representation was done by Newcombe et al. in 2011 [6]. Their system used a RGB-D sensor and generated a 3D voxelized grid Truncated Signed Distance Function (TSDF) of the environment. For this type of representation each cube contains the value of the distance to the nearest surface. The sign of the value is based on which side of the surface the cube is relative to the sensor. This work has been the most capable at dealing with extremely noisy data and dynamic scenes. However, due to memory constraints the method can only represent environments that are about the size of a 4m cube. Also, it must be ray traced in order to be visualized.

2.1.3 Surface

One of the first major works which created a surface representation of the environment in real-time was done by Martin and Thrun in 2002 [37]. Their method utilized an EM framework to fit plane models to 3D point cloud data. Polygon mesh elements were then easily assigned to each plane. The main drive behind this work was to generate a map of the environment that uses a low amount of memory. Their method worked well for structured environments. One of the major limitations of their method, and other methods that only mesh large planar sections, is that the representation will only consist of planar sections and not capture the fine detail of the environment. In 2004 Viejo and Cazorla [38] developed a methodology for generating a mesh that can contain more information of the environment than large planar sections. Due to this ability, they termed their method to be "unconstrained." Essentially their method was based on a 3D Delaunay triangulation algorithm. Giesen surveyed Delaunay triangulation methods in [39]. Viejo and Cazorla were not able to obtain real-time results and, in fact, it has been seen that it is extremely difficult to run a 3D Delaunay triangulation in real time because of the numerous amount of distance calculations that are needed. One of the next major advances came from Weingarten and Siegwart in 2006 [40]. Their work also created a mesh that was only capable of capturing large planar surfaces. However, they showed increased robustness. In 2007 Pollefeys et al. published a work with multiple researchers [41, 42]. They developed a large urban mapping system consisting of a vehicle and eight camera systems. The processing was carried out by multiple CPUs and optimized with Graphics Processing Unit (GPU) calculations. In their work they used the camera systems to generate depth maps. The set of depth maps was then fused to create a new smaller set of depth maps that were more accurate. The depth maps in the smaller set were more accurate because the error was averaged out by using near-by depth maps. The smaller set was then used by a triangulation procedure to create

a mesh of the environment. The mesh generation procedure was based on a work from 2002 by Pajarola et al. [43]. This method defines a mesh in the depth image. It starts from a very coarse mesh and continues to refine in areas of the depth image based on a confidence criteria. In the work of Weingarten and Siegwart these meshes which are defined for each fused depth image are then checked for overlaps and duplicates are removed to make a single large mesh. One of the major drawbacks of this approach is that the output mesh can not be adapted by measurements which come from revisited parts of the scene. Another major advancement came in 2008 from Poppinga et al. [44]. In this work they used a Time of Flight (ToF) camera to generate a mesh representation of the large planar structures in the environment. Here they also develop a procedure to determine a mesh in a depth image. They leverage the structure of the depth image to make the method computationally inexpensive. In their work they simply append the meshes which are created from each depth image into a global coordinate system. They obtain very good results from a simple method. Once again, the method is not adaptive to new information. Also, a mesh is created for each depth image instead of updating and maintaining a global mesh. A major advancement came from a famous work done by Newcombe and Davison in 2010 [45]. In this work they designed a method to create a mesh reconstruction from a single video camera. Their method used Structure From Motion (SFM) to obtain a sparse point cloud of the scene. Then an implicit function was fit to the point cloud using the methodology of Ohtake et al. [46]. A bundle of depth maps is then selected. From the bundle a single reference depth image is selected and a "base" model is constructed by sampling the implicit surface for vertices in the reference frame. The neighboring frames are used to better the "base" model and create a more accurate mesh. Each reference frame has its own mesh and all the meshes are put into a global coordinate system. Duplications are then detected and removed. Again, the representation is not adaptive to new information. In 2010 Stühmer et al. [47] advanced the field by publishing a method to generate very accurate depth maps

from several color images in real-time. They showed very impressive results but their method was not designed to maintain a representation in a global coordinate frame.

The next major advances in methods that generated surface representations of the environment, were based on RGB-D sensors. This type of sensor has become very popular since the release of the Kinect from Microsoft which was the first mass produced RGB-D sensor of its kind. RGB-D sensors are inexpensive and produce noisy 640x480 depth images at 30Hz. The RGB-D sensor has excited the robotics community because this has been the first time that depth data has been so readily accessible from such an inexpensive sensor. Therefore, these methodologies must be able to quickly deal with very high rates of information. One impressive work came from Henry et al. in 2012 [48]. In this work they designed a system which used a RGB-D sensor to build a map made of surfels (Surfels are circular disks which have a particular position and orientation and also a radial size based on confidence.). In order to generate and maintain the surfel map they used the work of Weise et al. [49]. The map consists of a large number of surfels. The surfel map can be updated given new registered depth images from the sensor. Decisions are made how to handle each measurement in the depth image based on the difference between an expectation generated using the current map and the actual readings from the sensor. Rendering a surfel map requires special methods [50] and is difficult to use in applications such as obstacle avoidance.

One of the next major advances is a highly-related work that was published by Whelan et al. in 2012 [51] and more recently in 2013 [52]. The system they developed was named Kintinuous and was able to produce a high quality mesh representation of the environment. Their hybrid system utilized the KinectFusion method [6] of Newcombe et al. to create a volumetric representation of the portion of the environment in front of the sensor. As the sensor moves, portions of the environment that leave the volume in front of the sensor are ray cast and turned into a mesh. They

obtain very impressive results but also mention a limitation of their system for future work. The limitation is that the mesh can not be updated once created, which is an issue when revisiting parts of the environment. One of the most impressive current works which has an adaptable mesh came from Cashier et al. in 2012 [53]. In this work, they were able to generate and update a mesh with new measurements from a ToF sensor. They used the difference between the existing model and the actual measurements to decide whether to adapt the mesh or add new elements. The mesh topology was not adaptive to the environment and their experiments only showed results of mapping a single flat wall with no robot movement. The system needs to be tested for object addition and removal.

2.2 Surface Reconstruction

The computer graphics field has spent considerable effort to develop methodologies for creating representations from sets of data. Generally, these sets of data are acquired from a sensor. Methodologies have progressed steadily and are often designed for a specific application. One of the original motivations was to generate surfaces from medical imaging data. This allows doctors to make better decisions because the data are presented in a more intuitive manner. Current applications include augmented reality and 3D printing. Older methodologies were not as concerned with speed and often times had a large computational cost. Also, the methodologies are often designed for single objects or small environments. Following the taxonomy of such well-known works as [54, 55], the field can be roughly divided into representations that are generated with volume-based techniques and those that use surface-based techniques. Methods that use volume-based techniques are characterized by spatially subdividing the environmental volume and are usually computationally expensive and require a large amount of memory. Methods that use surface-based

techniques generate the representation using surface properties of the input data. Both types of methods can have mechanisms to adapt the mesh to noisy or new information. In the following section we will trace the progression of the methodologies.

2.2.1 Volume-based

Volume-based methods spatially subdivide the volume into smaller parts and operations are performed on the mesh to either implicitly imply the surface or define the surface depending on the information contained in each subdivision. One of the first well-known works that used a volume-based technique was proposed by Lorensen and Cline in 1987 [3]. In this work they proposed a method named marching cubes which is still known for its reliability and simplicity and is used by applications which do not have a computational requirement. Marching cubes subdivides the space into cubes. The data contained in each cube dictate how the surface connectivity will be defined in that cube. Possible vertex locations are at the corners and along the edges. Once this has been done for all cubes the process is complete. One of the next major steps came from Hoppe et al. in 1992 [56] In this work they used the input points to define a Signed Distance Function (SDF) in 3D space and then meshed the zero-set to obtain the output mesh. A SDF is a spatial function which has the value of the distance to the nearest surface at each point. The sign is used to specify if the point is inside our outside of the surface relative to the sensor. The zero-set of the SDF is the surface where the values transition from positive to negative. Using a SDF has proven to be very effective and has been the core idea of many methodologies that came after this work of Hoppe et al., such as KinectFusion [6]. One of the next advances came from Edelsbrunner and Mücke in 1994 [57] with a method named alpha shapes. Here they used 3D Delaunay triangulation and the input point set to decompose the volume into a Delaunay tetrahedrization. This gives a triangulation

of the input set which involves all points. A sphere of radius alpha is then used to remove edges and vertices to obtain a mesh of user specified resolution. Many works have made use of 3D Delaunay triangulation to create a mesh. Methods which use 3D Delaunay on the input set have a large computational cost and often cannot be executed in real-time. The next valuable contribution came from Bloomenthal in 1994 [58] as open source software for surface polygonization of implicit functions. This was a stable and robust open source software that has been used in many well-known algorithms [45]. Another major advance came from Curless and Levoy in 1996 [59]. In this work they also constructed a Truncated Signed Distance Function (TSDF). A TSDF is very similar to a SDF, the only difference is that distance values are truncated after they exceed a certain threshold. Their method was one of the first to be able to handle several registered range scans. Their work showed how well a TSDF can deal with several noisy scans by naturally integrating out the error. They obtained very good results but not even close to real-time. A speed up in processing time was achieved by Pulli et al. in 1997 [60] by utilizing octrees. They obtained good results and their method was used by Surmann et al. [61] in a well-known robotic mapping work. Another major advance came in 2001 from Zhao et al [62]. They used Partial Differential Equation (PDE) methods to obtain a final reconstruction that was of better quality than prior methods. In 2001 Carr et al. [63] created a volumetric method based on the radial basis function (RBF). Their method was able to successfully deal with holes and generate water tight models. A water tight model is useful for single object reconstruction. However, it is not desired for mapping large environments. One of the next major advances was published in 2003 by Ohtake et al. [46]. In this work they created a method which was faster than the work of Carr et al. [63] by implementing a hierarchical approach with compactly supported basis functions. Their work has been considered to be the state of the art for calculating an implicit function of a noisy point set and was used by Newcombe et al. [45]. Volume-based methods have been able to create high quality represen-

tations and work well for single objects and small environments. These methods must spatially divide the environmental volume and therefore have a high memory requirement.

2.2.2 Surface-based

One of the first interesting and adaptive surface-based methods was published by Terzopoulos and Vasilescu in 1991 [64] and dealt with 2.5D data such as intensity and range images. The goal of their work was to create an adaptive mesh of an input image. The mesh was initialized as a 2D sheet of mesh elements with virtual springs along each edge. The stiffnesses of the virtual springs would then adjust based on the image information at that location. The mesh was able to adapt to be more dense in regions of higher intensity. In 1992 Terzopoulos and Vasilescu extended their methodology to 3D data [65]. In this work they used the distance between the mesh and the data to drive the vertices to be near the surface. In this early work they needed to initialize the mesh and control the subdivision of mesh elements to obtain a suitable resolution. In 1993 Hoppe et al. [66] published a method to optimize to resolution of a given mesh by posing the problem in an energy minimization framework. They minimized an energy function which tried to adequately represent the surface in the most concise mesh possible. One of the next advances in physical based adaptation of meshes came in 1993 from Huang and Goldof [67]. In this work they were able to adjust the size of the mesh elements to obtain a better resolution in areas of high frequency information using a physical based model. In addition, it was one of the first works to represent an object undergoing deformation. They method was able to perform tracking on simple simulation examples. Another advancement came in 1994 Rutishauser et al. [68] with a method specifically designed for incremental data. Their methodology worked with a sequential input set of range data and used a probabilistic framework to adjust the vertices of a mesh to the ex-

pected value given the prior observations. Their methodology also modeled the noise of the sensor with a sensor model. In 1994 Delingette [69] developed a methodology to generate a simplex mesh model of structured and unstructured 3D datasets. Elastic behavior of the mesh surface was modeled by local stabilizing functionals. Also, they implemented an iterative refinement process to refine the mesh in areas of high frequency information. One of the next steps was published by Turk and Levoy in 1994 [70]. Their method allowed overlapping meshes to be "zippered" into a single mesh surface. This ability is especially important for methods that generate a mesh for each depth image of the sensor and then need to combine all registered meshes into a single mesh. Their method is computationally expensive due to distance calculations. An interesting work came in 1995 from Chen and Medioni [71]. They devised an adaptive mesh methodology based on the inflation of a balloon. A mesh sphere was first initialized within the registered range measurements of the object. Virtual inflation forces were then used to expand the balloon until the mesh surface was a minimal distance from the range data. This method was limited to objects which are water tight. A major advancement came in 1999 from Bernardini et al., [72] in a method named the ball-pivoting algorithm. Their method is a good example of an advancing front method. These types of algorithms start with a seed mesh element and advance the boundary by adding new mesh elements in the immediate area of the boundary which is supported by measurements. Most advancing front algorithms differ in how it is decided to add new mesh elements. In the work of Bernardini et al. a virtual sphere of a user defined radius is rolled along the boundary of the mesh and new elements are added if the ball touches another measurement. Their methodology became popular because of its simplicity. One major disadvantage was that the generated mesh was a fixed topology. Another advancing front method came in 2001 from Gopi et al. [73, 54]. Here they sampled the input dataset to obtain a new dataset with a lower density of points in areas of lower frequency information. This effectively gave their method an adaptive topology. Next, a local

neighborhood was computed at each data point and projected to a plane tangent to the surface. The triangulation is then computed on this local tangent plane. They obtained impressive results on datasets of varying sample density and curvature. An interesting work was published in 2003 by Ivrissimtzis et al. [74]. Here they used a neural network model to adapt a mesh model to the data. They claimed that their method is computationally independent of the size of the input dataset because the dataset is only sampled by the method. There obtained good results. In 2004 Alexa et al. published a very interesting work to generate point set surfaces from an input dataset [75]. They use moving least squares (MLS) to locally approximate the surface with polynomials. The original dataset is then no longer used. Instead, they develop tools to sample the approximated surface to any resolution desired so that the end result is another point set of user specified resolution lying closer to the surface than the input dataset. One drawback is they had to develop their own methodology to render a point set. In 2005 Scheidegger et al. used the work of Alexa et al. to develop an advancing front methodology to generate concise meshes of high accuracy. Their main contribution was to augment an advancing front algorithm with global information so that the triangle size could adapt gracefully to any change. They obtained very impressive results. Most methodologies in Surface Reconstruction had been solely concerned with object or small environment recreation and have computational or memory requirements which do not work well with large environments. One of the first successful methods intended for large environments was published in 2009 by Marton et al. [76]. Their methodology was an advancing front algorithm which worked on a point set which was sampled from the MLS surface of the original point set. They were able to obtain impressive and near real-time results on datasets of large environments. They also developed a method to deal with revisited parts of the scene by determining the overlapping area and reconstructing only the updated part of the surface mesh. While this is a step forward, it would be better if the mesh surface converged to the actual surface with an increasing number of measurements.

To support dynamic scenes they developed mechanisms to decouple and reconstruct the mesh quickly. They only discussed these mechanisms in theory and had no results of how these mechanisms work. While Surface-based Surface Reconstruction techniques have developed impressively, several key issues arise when applying these techniques to mapping large environments.

2.3 Summary

The fields of Robotics and Computer Vision have developed many exciting methodologies to construct representations from a noisy input dataset. However there is still work to be done to obtain the ideal reconstruction method. A mesh is clearly a desirable type of representation. An ideal method should be able to generate and maintain a mesh representation efficiently. Also, many existing methods do not leverage the inherent structural information contained within the depth image. There are imaging processing techniques that could be used to answer some of the remaining problems in surface reconstruction, such as the need for adaptive topology and the need to decide how each measurement should be used to update the existing mesh. Henry et al. [48] has already investigated using the difference between the expected and actual measurements to guide the decision of how to use each measurement. However, their work was intended for surfels and needs to be extended to meshes. A method to generate a representation is needed which is computationally and memory efficient and can better adapt the representation to new information.

Chapter 3

Approach

3.1 Algorithmic Design

The algorithmic structure of MABDI can be seen in system diagram shown in Fig. 3.1. Table 3.1 gives a description of the main variables.

Table 3.1: Basic description of the main variables

Variable Name	Description
D	Depth image from RGB-D sensor
P	Pose of the sensor
D_n	Parts of D that are *novel*
S	Novel surface generated from D_n
M	Global mesh

The system diagram is very similar to Fig. 1.2 with the exception of the Classification component, shown in blue. This Classification component is MABDI's contribution to the state-of-art in mesh based mapping algorithms, and is what gives MABDI the ability to make decisions about the incoming data. The Classification component consists of two elements:

1. *Generate Expected Depth Image E* - Here we take the global mesh M, render it using computer graphics, and use the depth buffer of the render window to create a depth image E of what we expect to see from our sensor. This method requires the current pose P of the actual sensor (simulated for our experiments).

2. *Classify Depth Image D* - Here we classify the actual depth image D (simulated for our experiments) by first taking the absolute difference between E and D and thresholding. If the differences are small, those points are thrown away and if the differences are large, those points are kept as D_n. The idea behind this is, if the difference is large, the measurements are coming from a part of the environment that has not been seen before, i.e. novel. The implication of this assumption is that this version of MABDI cannot handle object removal. It is worth noting that MABDI can be extended to handle object removal by using the sign of the difference between E and D instead of the absolute value.

The system diagram in Fig. 3.1 also shows the Input and the Surface Reconstruction components. The Input component has been simulated for our experiments. More details of this simulation will be covered in Section 4. The Surface Reconstruction component of the MABDI algorithm can be implemented with any viable surface reconstruction method. Our implementation utilizes the structural information contained within the depth image. We will discuss this in more detail in the next section.

3.2 Implementation

3.2.1 Surface Reconstruction

A depth image is not simply a set of unorganized points, but has inherent structural information as well. This characteristic of the depth image allows us to define a topology on the 2 dimensional depth image that is preserved when projected to real-world coordinates. Our surface reconstruction method defines a topology that is visualized in Fig. 3.2. Here elements of the mesh are shown in light blue and novel points D_n are shown as blue dots. The red dot signifies a point that is not from the set D_n. Our implementation removes all mesh elements touching such points, as seen in the figure.

Our surface reconstruction methods was chosen for its ability to be implemented simply and run quickly. One consequence of our method is that the resulting surface S can have a large amount of elements. For example, if all points from D are classified as novel (this happens on the first frame), S can contain over $600,000$ elements. This assumes D has no invalid points, e.g., out of the sensor's range. Many surface reconstruction methods have been developed to create a surface more intelligently, as discussed in Section 2. For example, the advancing front method developed by Marton et al. [76] is capable of creating surfaces with fewer elements by utilizing robust resampling methods. One great thing about the MABDI algorithm is that the method developed by Marton et al. can be used in place of our surface reconstruction method. Also, due to our implementation's modular software design, the entire code base would not need to be changed in order to accomplish this. We will discuss the software design in the next section.

3.2.2 Software Design

From a software perspective, the major difficulty of implementing the MABDI algorithm was found to be creating both the simulated depth image D and the expected depth image E. In addition, managing the complexity of the data pipeline needed to run the algorithm and the simulation of the sensor proved to be difficult. Thankfully, Kitware, who is a leading edge developer of open-source software, created the Visualization Toolkit (VTK) [77, 78]. At the time of this writing the VTK Github repository has over 60,000 commits and is contributed to by supporters such as Sandia National Labs [79].

VTK is aptly designed for the implementation of MABDI for many reasons. Perhaps the most important is the concept of a vtkAlgorithm (often called a Filter). This allows a programmer to create a custom and modular processing pipeline by defining classes that inherit vtkAlgorithm and then defining the connections between these classes. For example, you could have a pipeline that reads an image from a source (component 1), performs edge detection (component 2), and then renders the image (component 3). Using this concept, the individual elements of MABDI can be succinctly defined in individual classes. With that in mind, we can see in Fig. 3.3 the layout used in my implementation of MABDI. Note, vtkImageData and vtkPolyData are VTK types used to represent an image and mesh respectively:

- *Source* - Classes with the prefix Source define the environment that is used for the simulation and provide a mesh in the form of a vtkPolyData.
- *FilterDepthImage* - Render the incoming vtkPolyData in a window and output the depth buffer from the window as a vtkImageData. The output additionally has pose information of the sensor.
- *FilterClassifier* - Implements the true innovation of MABDI, takes the differ-

ence between the two incoming depth images (vtkImageData) and outputs a new depth image where the data that is not novel is marked to be thrown away.

- *FilterDepthImageToSurface* - Performs surface reconstruction on the novel points. In this simple implementation the topology of the mesh is defined in the image coordinates and can be thought of as a checkerboard pattern with two triangles in every square. The data is then projected to real-world coordinates. The topology and the real-world coordinates are combined to define a surface and output as a vtkPolyData.

- *FilterWorldMesh* - Here we simply append the incoming novel surface to a growing global mesh that is also output as a vtkPolyData.

MABDI is implemented in Python and uses VTK. Our implementation is distributed under the BSD license and is available on Github at the address below:

$$https://github.com/lucasplus/MABDI$$

At the time of this writing, it consists of over 1,400 lines. The code that implements the MABDI algorithm itself is around 750 lines.

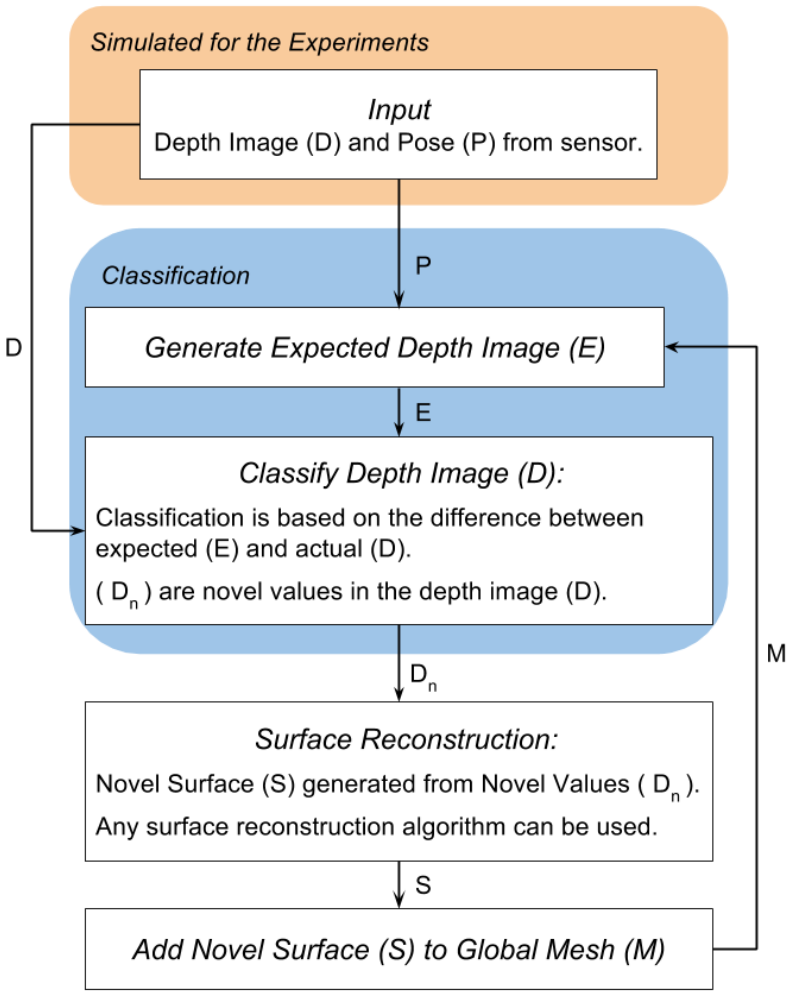

Figure 3.1: MABDI system diagram

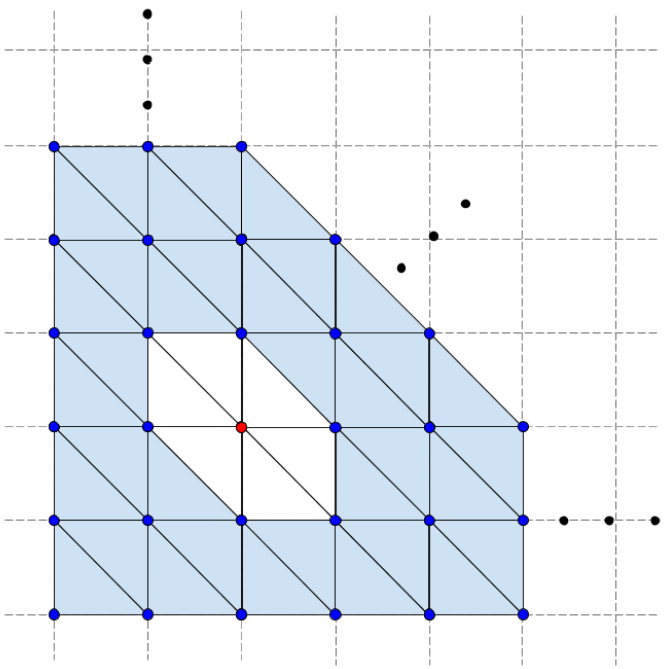

Figure 3.2: Surface reconstruction method

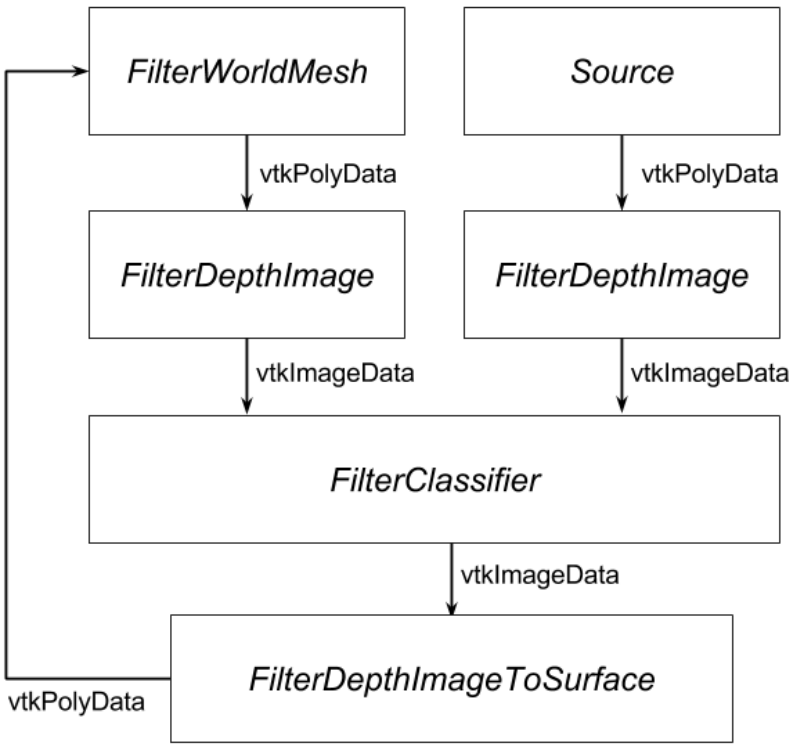

Figure 3.3: MABDI software diagram

Chapter 4

Experimental Setup

It was decided to develop and test MABDI in a completely simulated environment so that all results could be repeatable and also to facilitate the ability to debug during the development process. This ability was truly invaluable as some components of the algorithm proved to be complex from an implementation perspective. In addition, we can now compare the resultant global mesh to ground truth.

4.1 Simulation Parameters

The simulation was designed to be highly configurable and is implemented by a class named MabdiSimulate. The class is initialized with parameters that control all aspects of the simulation. Parameters of a particular importance are discussed in more detail here:

- Environment - This parameter specifies the environment used to generate the simulated depth images. *Table* is an environment consisting of a table and two cups placed on the table. The table is 1 meter tall. *Bunnies* is an environment

consisting of three bunnies who are around 1.5 meters tall. These bunnies are created using the Stanford Bunny [70], a well known data set in computer graphics.

- Noise - If true, adds noise to the depth image of the simulated sensor.
- Dynamic - If true, adds an object during the simulation. In the case of this analysis, a third bunny is added half-way through the simulation.
- Iterations - The number of iterations the simulation will have. This parameter affects the distance the sensor travels from frame to frame.

For this paper we will be exploring three experimental runs to demonstrate the ability of the MABDI implementation to generate valid results. Additionally, the experimental runs will be able to show the capabilities of the MABDI algorithm such as handling object addition in the environment.

Table 4.1: Description of the experimental runs.

	Environment	Noise	Dynamic	Iterations
Run 1	Table	False	False	30
Run 2	Bunnies	True	False	50
Run 3	Bunnies	True	True	50

All experimental runs define a helical path for the sensor to follow during the simulation. The path circles the objects in the environment twice. A helical path was chosen because it returns to a part of the environment that has been already mapped and is thus "known" to the global mesh. Also, because the path is a helix and not just a circle, the sensor views the environment from a slightly different position on each pass.

4.2 Analysis of Simulated Noise

In order to realistically simulate the sensor in a real-world environment we add noise to the depth image D. See Fig. 3.1. The magnitude of the noise added is based on the accuracy of real-world sensors. As new RGB-D sensors have been developed, such as the Asus Xtion and the Kinect for Xbox One, the accuracy of the sensors has continued to improve [80]. For this work, we take a conservative approach and utilize the well known error modeling work of Khoshelham [81] that is based on the original Kinect.

The depth image used by the MABDI algorithm E and the depth image that comes from simulating the environment D both use a pinhole camera model. This method has been validated in the localization work of Fallon [82]. The intrinsic camera parameters of the pinhole hole model were chosen to emulate the Kinect sensor [83]. The pinhole model defines a transformation matrix used to transform between viewpoint coordinates and real-world coordinates. The z component of the viewpoint coordinates constitutes the depth image and are defined to vary between 0 and 1. Due to how the transformation works, differences in the depth image do not linearly correspond to changes in real-world coordinates as can be seen in Fig. 4.1.

The noise added to D is defined by the equation below. The standard deviation σ=0.001 was chosen so that the resultant errors in the real-world coordinates would correlate to the error model in [81]. The text boxes in Fig. 4.1 show the resultant real-world error for two values of D; they match the error model of [81].

$$D_{noisy}(i,j) = D(i,j) + D(i,j) * \mathcal{N}(\mu{=}0, \sigma{=}0.001)$$

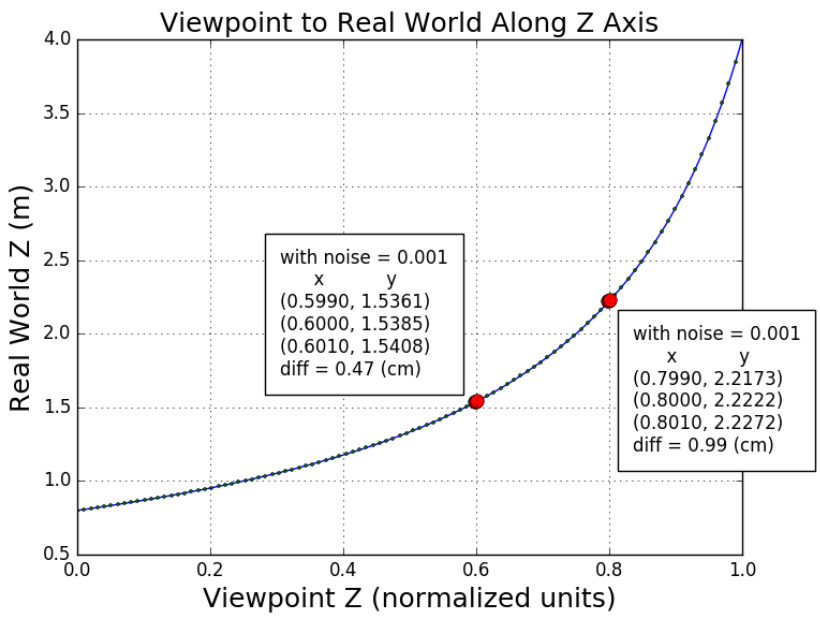

Figure 4.1: Viewpoint coordinates to real world coordinates analysis.

Chapter 5

Results

5.1. The figure shows a set of six views of information for each run. These views are created at every iteration and generate a movie of the run. Fig. 5.1 shows a snapshot of these views at different points of the simulation for each run. The views are described below:

- Top Left - View of the global mesh M from a third perspective. The wire frame corresponds to the viewing frustum of the sensor. The light blue helical line is the path of the sensor. Gray is the simulated environment. The multi-colored mesh is the global mesh M. The mesh is multi-colored in order to show the passage of time. For example, in Run1, The mesh is colored yellow, light green, and dark green for iterations 1, 2, and 3 respectively.

- Top Middle - Same as Top Left except it shows the novel surface S instead of the global mesh M.

- Top Right - Plot showing the number of elements in the global mesh M up to this iteration.

- Bottom Left and Bottom Middle - Actual D and expected E depth image respectively.

- Bottom Right - The classified depth image. Novel point D_n are shown in black. Points to be thrown away are shown in white.

We can notice important aspects of MABDI using Fig. 5.1. Notes on each of the runs:

- Run 1 - Top Left shows how the M gets composed over time. It is important to note that the mesh is not overlapping itself. This can be understood by noticing S from Top Middle is the same as the section of M this is colored dark green.

- Run 2 - This run shows clearly how the classification process is able to distinguish novel points. This can be seen by noticing the valley in-between the ear and the eye of the bunny closest to the sensor. The sensor was not able to see these points from the prior iteration due to occlusion. From the sensor's current perspective, the points can now be seen. Notice how the valley is missing in the *expected* depth image E, classified as novel in Bottom Right, and thus reconstructed into S. This is a clear example of the concept behind MABDI.

- Run 3 - This run shows how MABDI reacts to object addition. At this iteration the middle bunny is suddenly added. We can follow the data: D shows the new bunny, E shows what we expect to see (the middle bunny is not there because it is not in M), Bottom Right shows all points corresponding to the new bunny as marked as novel, and finally the novel points are reconstructed as S and appended to M. Top Right also shows a large jump in the number of elements in M due to the new bunny.

runs along with a plot of the number of elements in the mesh over iterations. These plots show the main contribution of MABDI because they level-off as the environment becomes more known as opposed to traditional "black box" reconstruction methods where the number of elements increases linearly over time.

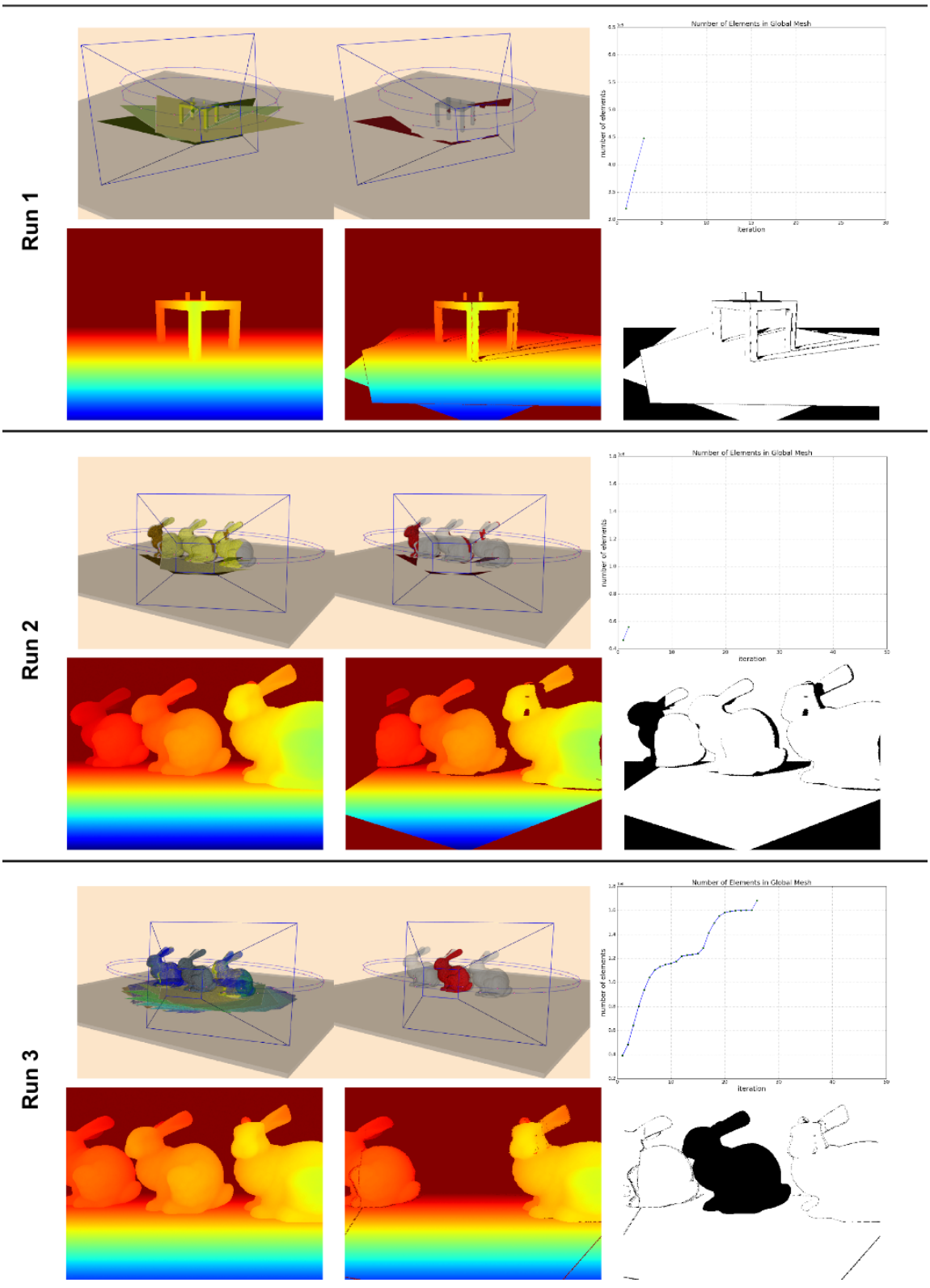

Figure 5.1: Results of all experimental runs. See Results Section for discussion.

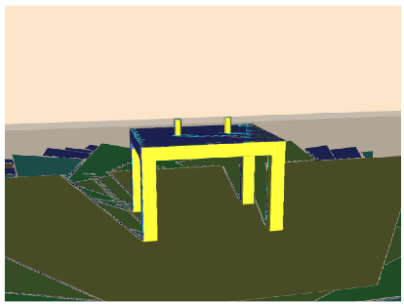

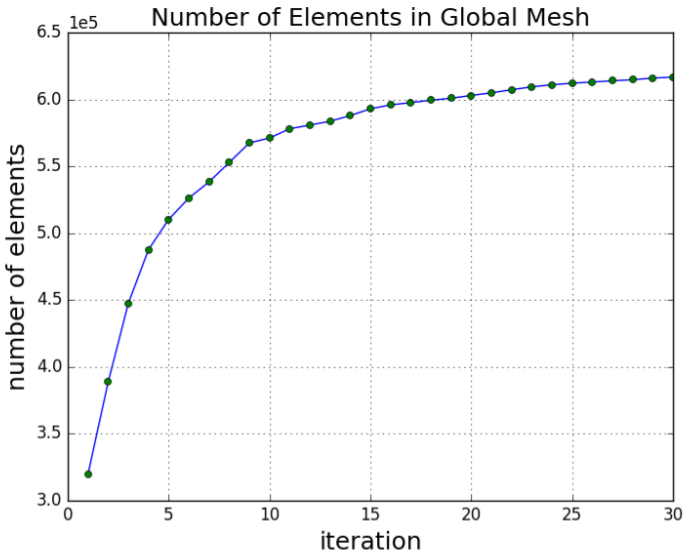
Number of Elements in Global Mesh
1e5
number of elements
iteration

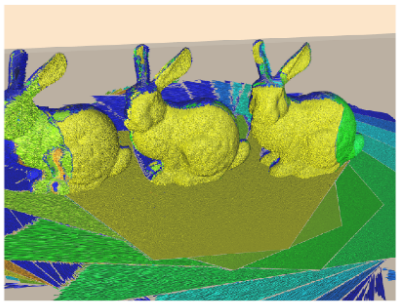

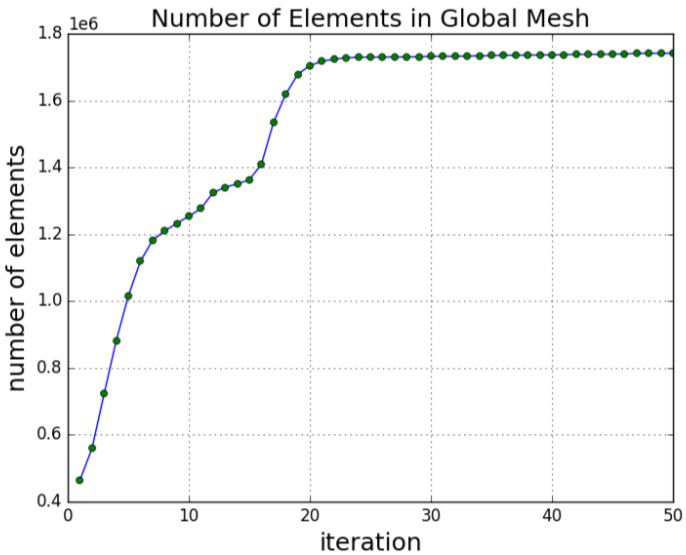
Number of Elements in Global Mesh
1e6
number of elements
iteration

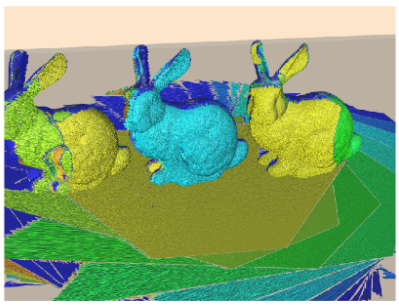

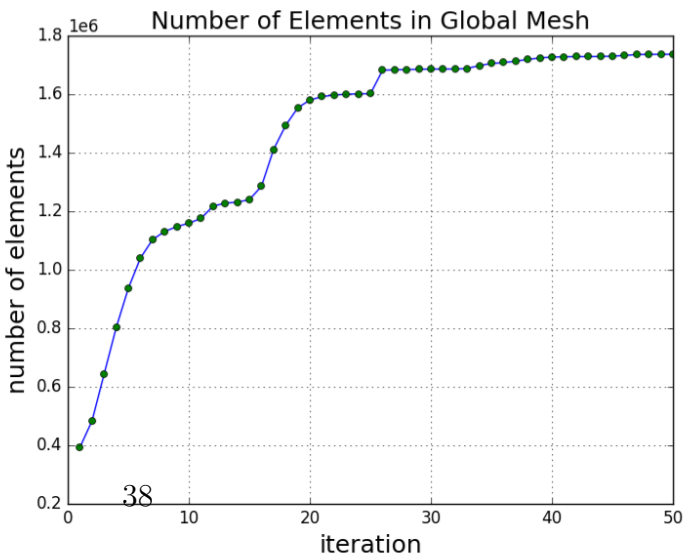
Number of Elements in Global Mesh
1e6
number of elements
iteration

Chapter 6

Conclusion

The goal of MABDI is to determine data from the sensor that has not yet been represented in the map and use this data to add to the map. MABDI does this by leveraging the difference between what we are actually seeing and what we expect to see. MABDI can work in conjunction with any "black box" mesh-based surface reconstruction algorithm, and can be thought of as a general means to provide introspection to those types of reconstruction methods.

The MABDI implementation was able to successfully perform in a realistic simulation environment. The results show how novel sensor data was successfully classified and used to add to the global mesh. Also, the MABDI algorithm runs at around 2Hz on a consumer grade laptop with an Intel i7 processor. This performance means that it is capable of real-world applications.

Currently MABDI is only designed to handle object addition, but the idea can be extended to handle both object addition and removal as discussed in Section 3.1. This would give the system the capability to handle highly dynamic environments such as a door opening and closing.

References

[1] M. W. Kadous, R. K.-M. Sheh, and C. Sammut, "Effective user interface design for rescue robotics," in *Proceeding of the 1st ACM SIGCHI/SIGART conference on Human-robot interaction - HRI '06*. New York, New York, USA: ACM Press, mar 2006, p. 250.

[2] S. Thrun, "Robotic mapping: A survey," *Exploring artificial intelligence in the new millennium*, no. February, 2002.

[3] W. E. Lorensen and H. E. Cline, "Marching cubes: A high resolution 3D surface construction algorithm," *Computer*, vol. 21, no. 4, pp. 163–169, 1987.

[4] B. Freedman, A. Shpunt, M. Machline, and Y. Arieli, "Depth mapping using projected patterns," 2012.

[5] P. Henry, M. Krainin, E. Herbst, X. Ren, and D. Fox, "RGB-D mapping: Using Kinect-style depth cameras for dense 3D modeling of indoor environments," *The International Journal of Robotics Research*, vol. 31, no. 5, pp. 647–663, apr 2012.

[6] R. A. Newcombe, S. Izadi, O. Hilliges, D. Molyneaux, D. Kim, A. J. Davison, P. Kohli, J. Shotton, S. Hodges, and A. Fitzgibbon, "KinectFusion: Real-time dense surface mapping and tracking," in *2011 10th IEEE International Symposium on Mixed and Augmented Reality, ISMAR 2011*. IEEE, oct 2011, pp. 127–136.

[7] L. Xia, C.-C. Chen, and J. K. Aggarwal, "Human detection using depth information by Kinect," in *CVPR 2011 WORKSHOPS*. IEEE, jun 2011, pp. 15–22.

[8] J. Stowers, M. Hayes, and A. Bainbridge-Smith, "Altitude control of a quadrotor helicopter using depth map from Microsoft Kinect sensor," in *2011 IEEE International Conference on Mechatronics*. IEEE, apr 2011, pp. 358–362.

[9] M. Dissanayake, P. Newman, S. Clark, H. Durrant-Whyte, and M. Csorba, "A solution to the simultaneous localization and map building (SLAM) problem," *IEEE Transactions on Robotics and Automation*, vol. 17, no. 3, pp. 229–241, jun 2001.

[10] H. Durrant-Whyte and T. Bailey, "Simultaneous localization and mapping: part I," *Robotics & Automation Magazine*, 2006.

[11] T. Bailey and H. Durrant-Whyte, "Simultaneous localization and mapping (SLAM): Part II," *Robotics & Automation Magazine*, no. September, 2006.

[12] R. Smith, M. Self, and P. Cheeseman, "Estimating uncertain spatial relationships in robotics," *Autonomous robot vehicles*, 1990.

[13] S. Thrun, W. Burgard, and D. Fox, "A Probabilistic Approach to Concurrent Mapping and Localization for Mobile Robots," *Autonomous Robots*, vol. 25, pp. 1–25, 1998.

[14] J. Gutmann and K. Konolige, "Incremental mapping of large cyclic environments," in *Proceedings 1999 IEEE International Symposium on Computational Intelligence in Robotics and Automation. CIRA'99 (Cat. No.99EX375)*. IEEE, 1999, pp. 318–325.

[15] S. Thrun, D. Fox, W. Burgard, and F. Dellaert, "Robust Monte Carlo localization for mobile robots," *Artificial Intelligence*, vol. 128, no. 1-2, pp. 99–141, may 2001.

[16] M. Montemerlo, S. Thrun, D. Koller, and B. Wegbreit, "FastSLAM: A factored solution to the simultaneous localization and mapping problem," *Proceedings of the National conference on Artificial Intelligence*, pp. 593–598, 2002.

[17] S. Thrun, W. Burgard, and D. Fox, "A real-time algorithm for mobile robot mapping with applications to multi-robot and 3D mapping," in *Proceedings 2000 ICRA. Millennium Conference. IEEE International Conference on Robotics and Automation. Symposia Proceedings (Cat. No.00CH37065)*, vol. 1. IEEE, 2000, pp. 321–328.

[18] Y. Liu and R. Emery, "Using EM to learn 3D models of indoor environments with mobile robots," in *Machine Learning-International Workshop Then Conference*, 2001.

[19] A. Davison, "Real-time simultaneous localisation and mapping with a single camera," in *Proceedings Ninth IEEE International Conference on Computer Vision*. IEEE, 2003, pp. 1403–1410 vol.2.

[20] S. Thrun, D. Hahnel, D. Ferguson, M. Montemerlo, R. Triebel, W. Burgard, C. Baker, Z. Omohundro, S. Thayer, and W. Whittaker, "A system for volumetric robotic mapping of abandoned mines," in *2003 IEEE International Conference on Robotics and Automation (Cat. No.03CH37422)*, vol. 3. IEEE, 2003, pp. 4270–4275.

[21] A. Howard, D. Wolf, and G. Sukhatme, "Towards 3D mapping in large urban environments," *2004 IEEE/RSJ International Conference on Intelligent Robots and Systems (IROS) (IEEE Cat. No.04CH37566)*, vol. 1, pp. 419–424, 2004.

[22] D. Cole and P. Newman, "Using laser range data for 3D SLAM in outdoor environments," in *Proceedings 2006 IEEE International Conference on Robotics and Automation, 2006. ICRA 2006.* IEEE, 2006, pp. 1556–1563.

[23] G. Klein and D. Murray, "Parallel Tracking and Mapping for Small AR Workspaces," in *2007 6th IEEE and ACM International Symposium on Mixed and Augmented Reality*. IEEE, nov 2007, pp. 1–10.

[24] L. Paz, P. Pinies, J. Tardos, and J. Neira, "Large-Scale 6-DOF SLAM With Stereo-in-Hand," *IEEE Transactions on Robotics*, vol. 24, no. 5, pp. 946–957, oct 2008.

[25] K. Konolige and M. Agrawal, "FrameSLAM: From Bundle Adjustment to Real-Time Visual Mapping," *IEEE Transactions on Robotics*, vol. 24, no. 5, pp. 1066–1077, oct 2008.

[26] H. Strasdat, J. Montiel, and A. Davison, "Scale drift-aware large scale monocular SLAM," *Proceedings of Robotics: Science and Systems (RSS). Vol. 2. No. 3. 2010*, 2010.

[27] N. Engelhard, F. Endres, and J. Hess, "Real-time 3D visual SLAM with a hand-held RGB-D camera," *Proc. of the RGB-D Workshop on 3D Perception in Robotics at the European Robotics Forum*, no. c, 2011.

[28] S. Rusinkiewicz and M. Levoy, "Efficient variants of the ICP algorithm," in *Proceedings Third International Conference on 3-D Digital Imaging and Modeling*. IEEE Comput. Soc, 2001, pp. 145–152.

[29] B. Yamauchi, A. Schultz, and W. Adams, "Mobile Robot Exploration and Map-Building with Continuous Localization," *Proceedings. 1998 IEEE International Conference on Robotics and Automation (Cat. No.98CH36146)*, vol. 4, no. May, pp. 3715–3720, 1998.

[30] A. Schultz and W. Adams, "Continuous localization using evidence grids," in *Proceedings. 1998 IEEE International Conference on Robotics and Automation (Cat. No.98CH36146)*, vol. 4. IEEE, 1998, pp. 2833–2839.

[31] R. Biswas, B. Limketkai, S. Sanner, and S. Thrun, "Towards object mapping in non-stationary environments with mobile robots," in *IEEE/RSJ International Conference on Intelligent Robots and System*, vol. 1. IEEE, 2002, pp. 1014–1019.

[32] A. Eliazar and R. Parr, "DP-SLAM 2.0," in *IEEE International Conference on Robotics and Automation, 2004. Proceedings. ICRA '04. 2004.* IEEE, 2004, pp. 1314–1320 Vol.2.

[33] M. Magnusson, A. Lilienthal, and T. Duckett, "Scan registration for autonomous mining vehicles using 3D-NDT," *Journal of Field Robotics*, vol. 24, no. 10, pp. 803–827, oct 2007.

[34] A. Nüchter, K. Lingemann, J. Hertzberg, and H. Surmann, "6D SLAM3D mapping outdoor environments," *Journal of Field Robotics*, vol. 24, no. 8-9, pp. 699–722, aug 2007.

[35] A. Huang, A. Bachrach, P. Henry, M. Krainin, D. Maturana, D. Fox, and R. Nicholas, "Visual odometry and mapping for autonomous flight using an RGB-D camera," pp. 1–16, 2011.

[36] F. Endres, J. Hess, N. Engelhard, J. Sturm, D. Cremers, and W. Burgard, "An evaluation of the RGB-D SLAM system," in *2012 IEEE International Conference on Robotics and Automation*, vol. 3, no. c, IEEE. IEEE, may 2012, pp. 1691–1696.

[37] C. Martin and S. Thrun, "Real-time acquisition of compact volumetric 3D maps with mobile robots," in *Proceedings 2002 IEEE International Conference on Robotics and Automation (Cat. No.02CH37292)*, vol. 1. IEEE, 2002, pp. 311–316.

[38] D. Viejo and M. Cazorla, "Unconstrained 3D-Mesh Generation Applied to Map Building," *Progress in Pattern Recognition, Image Analysis and Applications*, vol. 3287, pp. 161–207, 2004.

[39] F. Giesen, "Delaunay Triangulation Based Surface Reconstruction: Ideas and Algorithms," no. November, 2004.

[40] J. Weingarten and R. Siegwart, "3D SLAM using planar segments," in *2006 IEEE/RSJ International Conference on Intelligent Robots and Systems*. IEEE, oct 2006, pp. 3062–3067.

[41] A. Akbarzadeh, J.-M. Frahm, P. Mordohai, B. Clipp, C. Engels, D. Gallup, P. Merrell, M. Phelps, S. Sinha, B. Talton, L. Wang, Q. Yang, H. Stewenius, R. Yang, G. Welch, H. Towles, D. Nister, and M. Pollefeys, "Towards Urban 3D Reconstruction from Video," in *Third International Symposium on 3D Data Processing, Visualization, and Transmission (3DPVT'06)*. IEEE, jun 2006, pp. 1–8.

[42] M. Pollefeys, D. Nistér, J.-M. Frahm, A. Akbarzadeh, P. Mordohai, B. Clipp, C. Engels, D. Gallup, S.-J. Kim, P. Merrell, C. Salmi, S. Sinha, B. Talton, L. Wang, Q. Yang, H. Stewénius, R. Yang, G. Welch, and H. Towles, "Detailed Real-Time Urban 3D Reconstruction from Video," *International Journal of Computer Vision*, vol. 78, no. 2-3, pp. 143–167, oct 2007.

[43] R. Pajarola, Y. Meng, and M. Sainz, "Fast Depth-Image Meshing and Warping," no. 02, 2002.

[44] J. Poppinga, N. Vaskevicius, A. Birk, and K. Pathak, "Fast plane detection and polygonalization in noisy 3D range images," in *Intelligent Robots and Systems (IROS) 2008*. Ieee, sep 2008, pp. 3378–3383.

[45] R. A. Newcombe and A. J. Davison, "Live dense reconstruction with a single moving camera," in *2010 IEEE Computer Society Conference on Computer Vision and Pattern Recognition*. IEEE, jun 2010, pp. 1498–1505.

[46] Y. Ohtake, A. Belyaev, and H. Seidel, "A multi-scale approach to 3D scattered data interpolation with compactly supported basis functions," in *2003 Shape Modeling International.* IEEE Comput. Soc, 2003, pp. 153–161.

[47] J. Stühmer, S. Gumhold, and D. Cremers, "Real-time dense geometry from a handheld camera," *Pattern Recognition*, pp. 11–20, 2010.

[48] P. Henry, M. Krainin, E. Herbst, X. Ren, and D. Fox, "RGB-D Mapping: Using Depth Cameras for Dense 3D Modeling of Indoor Environments," *The International Journal of Robotics Research*, vol. 31, no. 5, pp. 647–663, feb 2012.

[49] T. Weise, T. Wismer, B. Leibe, and L. Van Gool, "In-hand scanning with online loop closure," *2009 IEEE 12th International Conference on Computer Vision Workshops, ICCV Workshops*, pp. 1630–1637, sep 2009.

[50] H. Pfister, M. Zwicker, J. van Baar, and M. Gross, "Surfels : Surface Elements as Rendering Primitives," in *SIGGRAPH 2000*. New York, New York, USA: ACM Press, jul 2000, pp. 335–342.

[51] T. Whelan, M. Kaess, and M. Fallon, "Kintinuous: Spatially Extended KinectFusion," 2012.

[52] T. Whelan, H. Johannsson, M. Kaess, J. J. Leonard, and J. B. McDonald, "Robust Tracking for Real-Time Dense RGB-D Mapping with Kintinuous," in *ICRA 2013*, no. MIT-CSAIL-TR-2012-031. Computer Science and Artificial Intelligence Laboratory, MIT, sep 2012.

[53] L.-K. Cahier, T. Ogata, and H. Okuno, "Incremental probabilistic geometry estimation for robot scene understanding," in *ICRA 2012*. Ieee, may 2012, pp. 3625–3630.

[54] M. Gopi and S. Krishnan, "A fast and efficient projection-based approach for surface reconstruction," in *SIBGRAPI'02*, 2002, pp. 0–7.

[55] R. Mencl and H. Muller, "Interpolation and approximation of surfaces from three-dimensional scattered data points," *Scientific Visualization Conference, 1997*, 1997.

[56] H. Hoppe, T. DeRose, and T. Duchamp, *Surface reconstruction from unorganized points*, 1992, no. July 1992.

[57] H. Edelsbrunner and E. P. Mücke, "Three-dimensional alpha shapes," *ACM Transactions on Graphics*, vol. 13, no. 1, pp. 43–72, jan 1994.

[58] J. Bloomenthal, "An Implicit Surface Polygonizer," *In Graphics Gems IV*, pp. 324–349, 1994.

[59] B. Curless and M. Levoy, "A volumetric method for building complex models from range images," in *SIGGRAPH '96*, 1996, pp. 303–312.

[60] K. Pulli, T. Duchamp, H. Hoppe, J. McDonald, L. Shapiro, and W. Stuetzle, "Robust meshes from multiple range maps," in *International Conference on Recent Advances in 3-D Digital Imaging and Modeling*. IEEE Comput. Soc. Press, 1997, pp. 205–211.

[61] H. Surmann, A. Nüchter, and J. Hertzberg, "An autonomous mobile robot with a 3D laser range finder for 3D exploration and digitalization of indoor environments," *Robotics and Autonomous Systems*, vol. 45, no. 3-4, pp. 181–198, dec 2003.

[62] H. Zhao, S. Osher, and R. Fedkiw, "Fast surface reconstruction using the level set method," in *Variational and Level Set Methods in Computer Vision, 2001*, 2001, pp. 0–7.

[63] J. C. Carr, R. K. Beatson, J. B. Cherrie, T. J. Mitchell, W. R. Fright, B. C. McCallum, and T. R. Evans, "Reconstruction and representation of 3D objects with radial basis functions," *SIGGRAPH '01*, pp. 67–76, 2001.

[64] D. Terzopoulos and M. Vasilescu, "Sampling and Reconstruction with Adaptive Meshes," in *Computer Vision and Pattern Recognition, 1991. Proceedings CVPR '91.*, 1991.

[65] M. Vasilescu and D. Terzopoulos, "Adaptive meshes and shells: irregular triangulation, discontinuities, and hierarchical subdivision," in *Computer Vision and Pattern Recognition*, no. 1. IEEE Comput. Soc. Press, 1992, pp. 3–6.

[66] H. Hoppe, T. DeRose, T. Duchamp, J. McDonald, and W. Stuetzle, "Mesh Optimization," in *Proceedings of the 20th annual conference on Computer graphics and interactive techniques*, ser. SIGGRAPH '93, vol. d. New York, NY, USA: ACM, 1993, pp. 19–25.

[67] W.-C. Huang and D. Goldgof, "Adaptive-size meshes for rigid and nonrigid shape analysis and synthesis," *IEEE Transactions on Pattern Analysis and Machine Intelligence*, vol. 15, no. 6, pp. 611–616, jun 1993.

[68] M. Rutishauser, M. Stricker, and M. Trobina, "Merging range images of arbitrarily shaped objects," *Proceedings of IEEE Conference on Computer Vision and Pattern Recognition CVPR-94*, pp. 573–580, 1994.

[69] H. Delingette, "Simplex meshes: a general representation for 3D shape reconstruction," in *Computer Vision and Pattern Recognition*, 1994, pp. 856–859.

[70] G. Turk and M. Levoy, "Zippered polygon meshes from range images," in *SIGGRAPH '94*. New York, New York, USA: ACM Press, 1994, pp. 311–318.

[71] Y. Chen and G. Medioni, "Description of Complex Objects from Multiple Range Images Using an Inflating Balloon Model," *Computer Vision and Image Understanding*, vol. 61, no. 3, pp. 325–334, may 1995.

[72] F. Bernardini, J. Mittleman, H. Rushmeier, C. Silva, and G. Taubin, "The ball-pivoting algorithm for surface reconstruction," *IEEE Transactions on Visualization and Computer Graphics*, vol. 5, no. 4, pp. 349–359, 1999.

[73] M. Gopi, S. Krishnan, and C. Silva, "Surface reconstruction based on lower dimensional localized Delaunay triangulation," *Computer Graphics Forum*, vol. 19, no. 3, 2001.

[74] I. Ivrissimtzis, W.-K. Jeong, and H.-P. Seidel, "Using growing cell structures for surface reconstruction," *2003 Shape Modeling International.*, vol. 2003, pp. 78–86, 2003.

[75] M. Alexa, J. Behr, D. Cohen-Or, S. Fleishman, D. Levin, and C. Silva, "Point set surfaces," *Proceedings Visualization, 2001. VIS '01.*, pp. 21–537, 2004.

[76] Z. C. Marton, R. B. Rusu, and M. Beetz, "On fast surface reconstruction methods for large and noisy point clouds," in *2009 IEEE International Conference on Robotics and Automation*. IEEE, may 2009, pp. 3218–3223.

[77] W. J. Schroeder, B. Lorensen, and K. Martin, *The Visualization Toolkit*, 4th ed. Kitware, 2006.

[78] Kitware. (2016) VTK The Visualization Toolkit. [Online]. Available: http://www.vtk.org/overview/

[79] S. N. Labs. (2016) SNL Computational Systems and Software Environment. [Online]. Available: http://www.sandia.gov/asc/computational_systems/

[80] E. Lachat, H. Macher, M. A. Mittet, T. Landes, and P. Grussenmeyer, "First experiences with Kinect v2 sensor for close range 3D modelling," *The International Archives of Photogrammetry, Remote Sensing and Spatial Information Sciences*, vol. 40, no. 5, p. 93, 2015.

[81] K. Khoshelham and S. O. Elberink, "Accuracy and resolution of Kinect depth data for indoor mapping applications." *Sensors (Basel, Switzerland)*, vol. 12, no. 2, pp. 1437–54, 2012.

[82] M. F. Fallon, H. Johannsson, and J. J. Leonard, "Efficient Scene Simulation for Robust Monte Carlo Localization using an RGB-D Camera," in *2012 IEEE International Conference on Robotics and Automation*. IEEE, may 2012, pp. 1663–1670.

[83] Microsoft. (2016) Microsoft Robotics Kinect Sensor. [Online]. Available: https://msdn.microsoft.com/en-us/library/hh438998.aspx